Journal of Hydraulic Structures
J. Hydraul. Struct., 2024;9(4):88-113
DOI: 10.22055/JHS.2024.45888.1284

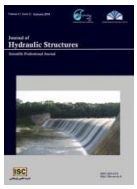

Conducting experimental and numerical studies to analyze the impact of the base nose shape on flow hydraulics in PKW weir using FLOW-3D

Behshad Mardasi [1]
Rasoul Ilkhanipour Zeynali [2]
Majid Heydari [3]

Abstract

Weirs are essential structures used to manage excess water flow from behind dams to downstream areas. Enhancing discharge efficiency often involves extending the effective length of Piano Key Weirs (PKW) in dams or regulating flow within irrigation and drainage networks. This study employed both numerical and laboratory investigations to assess the impact of different base nose shapes installed beneath the outlet keys and varying Input to output key width ratios (Wi/Wo) on discharges ranging from 5 to 80 liters per second. Furthermore, the study aimed to achieve research objectives and compare the performance of Piano Key Weirs with Ogee Weir. For numerical simulation, the optimal number of cells for meshing was determined, and an appropriate turbulence model was selected. The results indicated that the numerical model accurately simulated the laboratory sample with a high degree of precision. Moreover, the numerical model closely approximated PKW for all parameters Q, H, and Cd compared to the laboratory sample. The findings revealed that in laboratory models with a maximum discharge area of 80 liters per second, the weir with Wi/Wo=1.2 and a flow head value of 285 mm exhibited the lowest value, whereas the weir with Wi/Wo=0.71 and a flow head value of 305 mm showed the highest, attributed to the higher discharge in the input-output ratio. Additionally, as the ratio of flow head to weir height H/P increased, the discharge coefficient Cd decreased. Comparing the flow conditions in weirs with different base nose shapes, it was observed that the weir with a spindle nose shape (PKW1.2S) outperformed the PKW with a flat (PKW1.2), semi-cylindrical (PKW1.2CL) and triangular base nose (PKW1.2TR). The results emphasized that models featuring semi-cylindrical and flat noses exhibited notable flow deviation and abrupt disruption upon impact with the nose. However, this effect was significantly reduced in models equipped with triangular and spindle-shaped noses. Also, the coefficient of discharge in PKW1.2S and PKW1.2TR weirs, compared to the PKW1.20 weir, increased by 27% and 20%, respectively.

Keywords: Piano Key Weir, Base Nose Shape, Flow Hydraulics, Numerical Model, Triangular Nose Shape, Flat Nose Shape, Semi-Cylindrical Nose Shape, Spindle Nose Shape

Received: 18 January 2024; Accepted: 11 March 2024

[1] Department of Water Engineering, Faculty of Agriculture, Urmia University, Urmia, Iran. E-mail: bmardasi@yahoo.com **(Corresponding Author)**
[2] Department of Water Engineering, Faculty of Agriculture, Urmia University, Urmia, Iran.
[3] Department of Irrigation, Faculty of Agriculture, Bu-AliSina University, Hamedan, Iran.

1. Introduction

Constructing barriers along the flow path of rivers or waterways to redirect water for agricultural or drinking purposes has been a crucial human activity throughout history. A weir, by definition, is any structure placed in the direction of the flow that causes water to rise above the structure. Weirs are commonly used in irrigation and drainage canals to measure discharge and control the flow of water [1]. Weirs incorporated in dams serve the dual purpose of managing excess flow during floods and regulating the water level of the reservoir. However, the flow over weirs faces two primary challenges. The insufficient capacity of the weir to discharge water and the destructive effects of sedimentation. Reports on dam damage indicate that nearly 30% of these problems stem from the weirs' inadequate discharge capacity and resultant damage to the structures. Consequently, the International Committee on Large Dams (ICOLD) recommends a thorough re-examination of high dam weirs to ensure their safety and integrity [2]. As a consequence, many dams require rehabilitation to meet the more stringent criteria for dam safety [3]. Piano Key Weirs (PKW) are a contemporary variation of long crest weirs. Their unique geometric design enables installation on the crests of numerous existing dams. PKW offer an optimal solution for upgrading existing weir structures, being both cost-effective and capable of enhancing reservoir capacity. Moreover, they have the added benefit of augmenting flood discharge capabilities [4]. PKW significantly enhances flow under low head conditions and, by aerating the flow, reduces the risk of cavitation. The first PKW was designed in 2001 by Lempérière and Blanc [5], marking a significant innovation in weir technology. This design quickly gained popularity and has been adopted worldwide [6]. A typical PKW comprises a sequence of identical rectangular keys, each featuring a sloping base that initially slopes towards the flow and then diverges away from the crest of the weir. This alternating design enables the PKW to retain a narrower base compared to conventional labyrinth weirs [7]. Two fundamental factors affecting the efficiency of the weir are the direction of the inlet flow relative to the symmetry axis of the weir and the configuration of the lateral transformation towards the inlet channel area of the weir [8]. The most suitable approach for studying and assessing these types of weirs involves constructing a laboratory physical model at a suitable scale. This model would feature a weir installed in a laboratory flume under sub-critical flow conditions. The data obtained from such experiments can offer adequate accuracy for utilization in the preliminary design phases. However, for the final design, it becomes imperative to construct a physical model based on the findings of the preliminary design phase and subject it to more meticulous evaluation [9]. Erpicum et al. [10] delved into the discharge coefficient for PKW through meticulous analysis of laboratory data and the construction of diverse physical models. Similarly, Kabiri-Samani and Javaheri [11] explored various laboratory models to present discharge coefficients under both submerged and free-flow conditions. Hien et al. [12] investigated PKW across different types, determining that for type A weirs, efficiency is heightened with a low absorption ratio (H/P) at a value of n=7 (where n represents the number of weir cycles). For higher ratios, n=5 and 6 were found to enhance weir efficiency. Additionally, their findings suggested that the optimal number of cycles for types A and B weirs is n=6, with the most favorable W_i/W_0 ratio predicted to be 1.20. Contributing to this research, Machiels [4] scrutinized pressure, velocity, and flow profiles on asymmetric weirs, offering equations to compute discharge at the inlet, outlet, and lateral crest. Given the multifaceted nature of factors influencing the geometry and flow dynamics of these weirs, extensive studies are imperative [12 ,13, 14]. Basson et al. [15] provided a comprehensive overview of the intricate flow patterns and hydrodynamic phenomena associated with PKW. In a related study, Anderson and Tullis [16] investigated these weirs at two different scales, revealing significant effects of surface tension,

viscosity, and inertia on the flow's oscillatory behavior across various scales, in line with expectations. Furthermore, the research by Erpicum et al. [17] complements these studies by conducting a detailed examination of hydraulic behavior. Their primary focus was on optimizing discharge efficiency, which correlates well with earlier findings. Additionally, Emiroglu and Aydin [18] carried out an in-depth analysis of the overflow discharge capacity of lateral congress weirs. They discovered that the discharge rates predicted by Computational Fluid Dynamics (CFD) closely matched those observed in laboratory experiments across different flow scenarios. Expanding on this finding, Cicero et al. [19] focused specifically on Type A piano key weirs, using a numerical model for their simulation. Their study emphasized the effectiveness of three-dimensional flow models in accurately predicting the hydraulic performance of this type of weir, with an approximate error margin of 8%. While the impact of the base nose shape on weir efficiency has not received much attention, this research aims to address this gap by investigating how the shape of the base nose in the upstream outlet key affects the hydraulics of Piano Key Weirs, alongside exploring different ratios of the width of the inlet key to the width of the outlet key. To explore these aspects, various base configurations were tested in a physical model. These configurations included flat nose shapes (used as a control), as well as triangular and semi-cylindrical shapes. Additionally, Model A incorporated triangular and spindle shaped nose bases in the upstream outlet keys to further investigate their influence.

2. Materials and methods:

2.1. Dimensional analysis:

According to the studies conducted on PKW and the samples studied in this research, the parameters affecting the weir flow for the free flow state can be presented in the form of the following function:

$$Q = f(H, L, P, W, Wi, Wo, B, Bi, Bo, Ha, Hm, g, \rho, \sigma, \mu) \quad (1)$$

Where:

Q: Discharge Capacity
H: Total Upstream Head
L: Crest Centerline Length
P: Total Weir Height
W: Weir Width
W_i: Inlet Key Width
W_o: Outlet Key Width
B: The Lateral Weir Crest Length
B_i: Upstream Key Cantilever Lengths
B_o: Downstream Key Cantilever Lengths
H_a: Head Level of Flow in Test Weir (Control)
H_m: Head Level of Flow in Different Base Nose Shape
g: Acceleration due to Gravity
ρ: Water Density
σ: Surface Tension
μ: Dynamic Viscosity

These parameters, collectively describing the geometric characteristics of the weir and the properties of the fluid, can be analyzed using dimensional analysis techniques, specifically Buckingham's theory. The resulting dimensionless groups can be expressed in the following equations:

$$C_d = \varphi(\frac{H}{P}, \frac{L}{W}, \frac{B}{P}, \frac{W_i}{W_o}, \frac{B_i}{B}, \frac{B_o}{B}, \frac{H_a}{H_m}, We, Re) \quad (2)$$

Due to the negligible effect of viscosity compared to gravity-induced turbulence, the Reynolds number (Re) is omitted from the equation. Additionally, if the upstream flow head exceeds 3 cm (H>3 cm), the impact of surface tension is considered insignificant, and the Weber number (We) is excluded from the analysis. Thus, the relationship is summarized as follows:

$$C_d = \varphi(\frac{H}{P}, \frac{L}{W}, \frac{B}{P}, \frac{W_i}{W_o}, \frac{B_i}{B}, \frac{B_o}{B}, \frac{B_i}{B_o}, \frac{H_a}{H_m}) \quad (3)$$

In this context, the parameter H represents a hydraulic variable including the flow height on the crest and head, equivalent to the kinetic energy (velocity) upstream of the weir. The discharge coefficient (C_d) serves as a representation of the Froude number and hydraulic characteristics of the flow. The values of L/W and W_i/W_o are determined based on the width of the flume and optimal values suggested in various sources [3]. As the researched weir is of type A, the ratio B_i/B_o is set to 1. Additionally, the ratios B_i/B and B_o/B are held constant.

Table (1) presents a comprehensive comparison of the dimensions of overflows as constructed in both the physical model and the FLOW 3D numerical model.

Weir Model	W_i/W_o	$B_i=B_o$	L	P	W	W_i	W_o	B	D
	Input to output width ratio	Cantilever lengths	Crest centerline length	Total weir height	Key width	Inlet key width	Outlet key width	Weir length	Base diameter
PKW1	1	14	462	24	83	9.77	9.77	20	9.77
PKW1.2	1.2	14	462	24	83	10.7	8.9	20	8.9
PKW1.4	1.4	14	462	24	83	11.4	8.15	20	8.15
PKW0.83	0.83	14	462	24	83	8.9	10.7	20	10.7
PKW0.71	0.71	14	462	24	83	8.15	11.4	20	11.4
PKW1.2CL	1.2	14	462	24	83	10.7	8.9	20	8.9
PKW1.2TR	1.2	14	462	24	83	10.7	8.9	20	8.9
PKW1.2S	1.2	14	462	24	83	10.7	8.9	20	8.9

Table (2) provides detailed specifications of the dimensions of overflows constructed in the physical model, specifically focusing on the control model.

Control weir dimensions (A)			
P	24 cm	B	48 cm
L	462 cm	B	20 cm
W	83 cm	B_i	14 cm
W_o	10.7 cm	B_o	14 cm
W_i	8.9 cm	T	0.6 cm

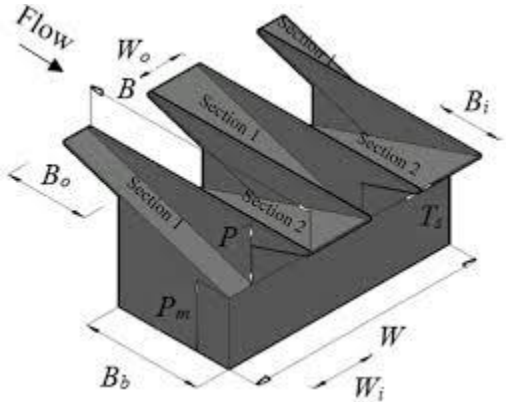

Figure (1) depicts a three-dimensional view of piano key overflows, complete with detailed geometrical parameters. PKW schematic diagram [4]

Laboratory Equipment: The experiments central to this study were conducted in the hydraulic laboratory of the Water Engineering Department at Bou Ali Sina University, equipped with glass walls and a stainless-steel floor for optimal observation and durability. To facilitate high-flow experiments, the laboratory's flume was designed with a unique structure, initially utilizing basic tools like plastic pipes for flow calming and water level control at the weir.

Water Flow System: A robust centrifugal pump, boasting a 15-kilowatt capacity, was tasked with pumping water into a sizable head tank (230 x 145 x 90 cm). The water, upon reaching a predetermined height in the tank, flowed into the laboratory flume, cascaded over the weirs, and was then recirculated back into the system, thereby creating an efficient closed-loop water recycling system.

Model Construction: The Piano Key Weir (PKW) models were meticulously crafted from 0.6 cm thick Plexiglas plates, shaped to precision with laser cutting, joined using drop glue, and sealed with silicone glue to prevent leaks. Water level readings were accurately captured using a point depth finder mounted on the flume.

Flow Measurement: Discharge measurements were precisely taken with a digital ultrasonic flow meter, calibrated against the water height on a 1-meter-wide rectangular weir at the flume's end. All PKW models were constructed with 4 cycles to maintain consistency.

Experimental Setup: The PKW weir was strategically placed 1.50 meters from the flume's downstream end and roughly 7 meters from the flow calming system. Experiments were conducted at specific discharges, with water level profiles measured approximately 2.5 meters upstream of the weir.

Numerical Simulation: The 3D models of PKW were initially designed using SketchUp software and then transferred to Flow 3D software with specialized STL format.All parameters and conditions used in the simulations were kept consistent with those employed in the physical experiments. This included maintaining the same fluid type and physical characteristics, arranging the mesh cells similarly, utilizing the same turbulence model, and employing identical time steps.
The analysis was performed within the Flow 3D software under steady flow conditions, with flow rates ranging from 5 to 80 liters per second for the weirs.

Optimization and Validation: The numerical model's ability to predict the flow coefficient, water level, discharge, and the relationship between discharge (Q) and height level (H) was investigated. The condition of the flow (free or submerged) was also controlled in each experiment.

Visual Representations: Table 1 provides the main dimensions of the constructed weirs, and Figure 1 illustrates the schematic of the weir.

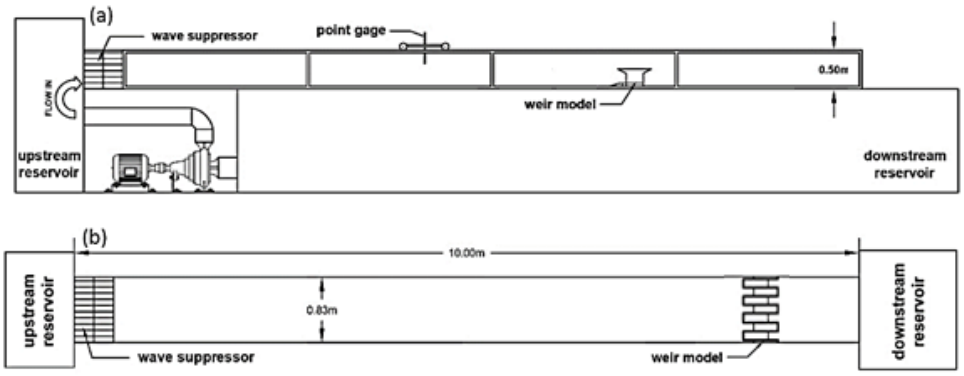

Figure (2): presents a detailed schematic of the physical model, illustrating the precise arrangement and location of the overflow structure and flume equipment.

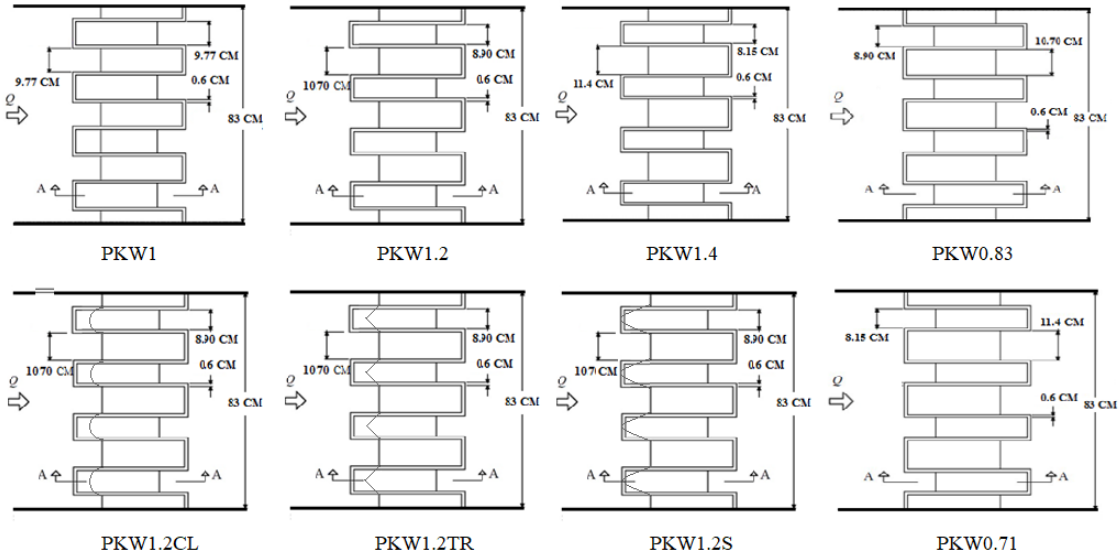

Figure (3): The weir form of the Piano Key Weir with the different base noses shape

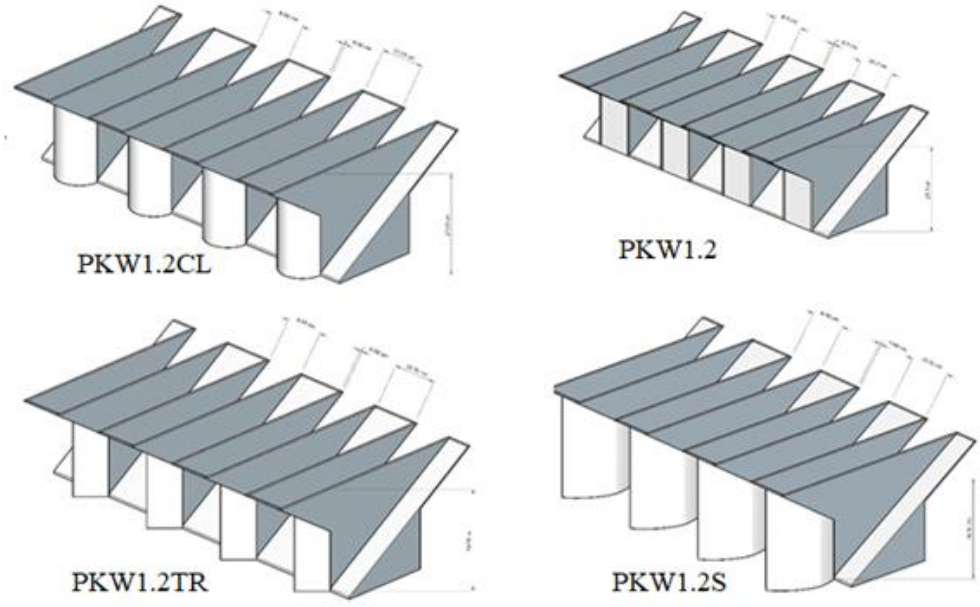

Figure (4): Schematic Representation of PKW with base noses shape, Showcasing Variations in Nose Designs

3. Discussion:

In this section, we examine the hydraulic conditions of flow in each piano key weir with various nose base shapes installed under the outlet key, considering both the physical model and the 3D numerical model.

Figure (5) illustrates a comparative analysis of the discharge performance of piano key weirs with a flat front and a series of peaks. The graph presents different models for flat nose shape and compares them with a series of piano keys and Ogee weir.

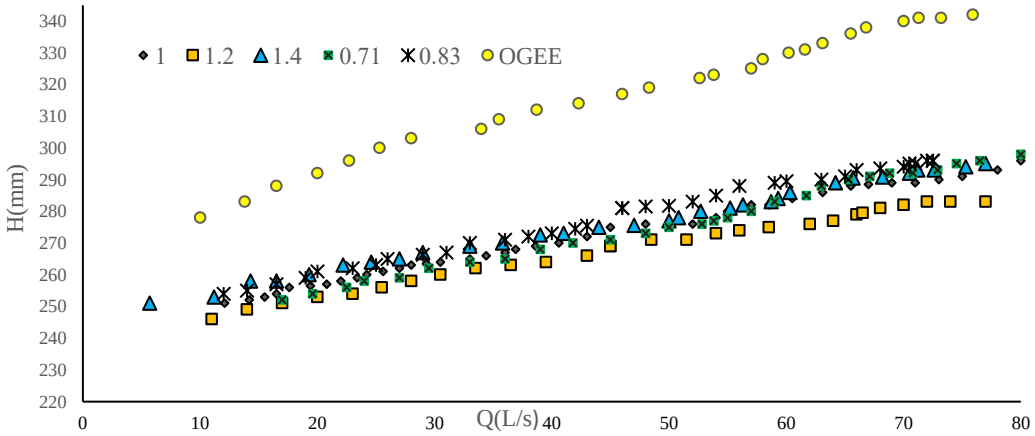

Figure (5): Comparison of the Discharge Performance of Piano Key Weirs

3.1. Selection of PKW1.2 Model for Further Analysis:

Considering the discharge coefficient, it can be seen that among the examined models, the PKW1.2 model exhibits the highest discharge coefficient. Therefore, this model is chosen as the model of choice to investigate other physical parameters.

The results obtained from the comparison graphs in Figure (4) reveal that, for laboratory models with a maximum discharge of 80 liters per second, the PKW1.2 discharge with a 285 mm level has the lowest discharge, while the PKW 0.71 with a 298 mm exhibits the highest. This discrepancy is attributed to the high-water discharge, leading to an elevated ratio of input to output current. An essential observation is that the maximum discharge in the lower head of the PKW1.2 model aligns with the findings of Anderson [20] at the University of Utah. This consistency is not only observed in the laboratory samples but is also evident in the numerical model.

3.2. Performance of PKW1.2 Weir:

Furthermore, the rate of discharge increases due to the rise in head in the PKW1.2 weir surpasses that of other weirs. This faster increase indicates superior performance compared to alternative weirs. Remarkably, the results obtained from numerical models regarding the percentage increase in head and discharge align with the trends observed in laboratory samples, reinforcing the reliability of the findings.

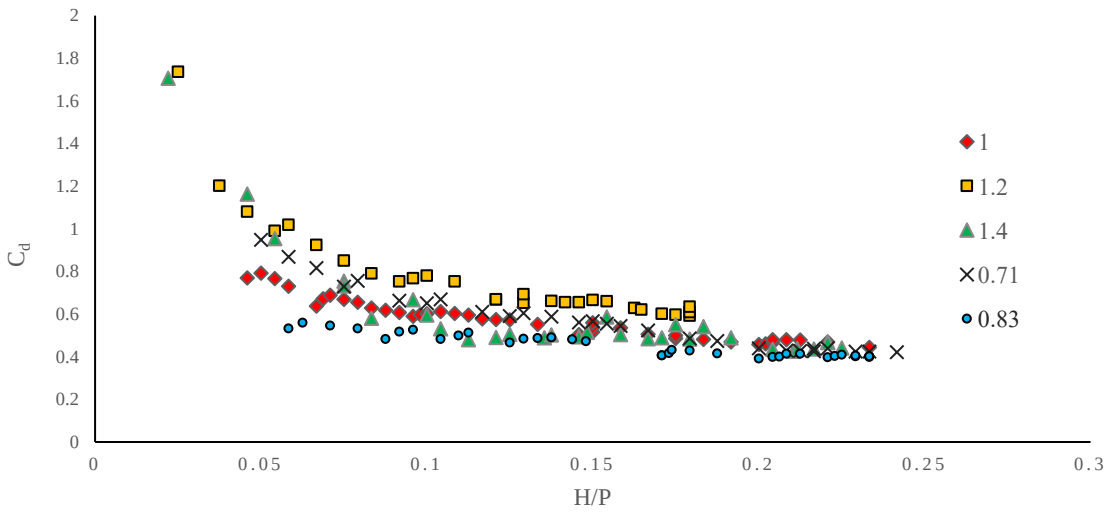

Figure (6): Comparison of the Discharge Coefficient (C_d) with the H/P in Laboratory Model Piano Key Weirs

In Figure 6, a comparison of the discharge coefficient (C_d) with the H/P submerged ratio in the laboratory model of piano key weirs has been presented. The results indicate that, overall, the discharge coefficient decreases with an increase in H/P. For the laboratory models, considering the maximum H/P, the PKW1.2 weir exhibited the highest discharge coefficient, while the PKW0.83 had the lowest discharge coefficient. This observation is attributed to the high-water discharge of the base with a substantial ratio of input to output. The importance of the maximum discharge of the PKW1.2 model aligns with the findings of Anderson at the University of Utah [20]. Andersen suggested that W_i/W_o=1.20-1.5 represents the optimal state for piano key weirs. By comparing the discharge coefficient between the PKW1.2 and PKW1.4 weirs, it was observed that these two weirs demonstrated similar efficiency, likely due to the balance between the width of the inlet cycle and the width of the outlet cycle concerning hydraulic capacity.

3.3. Effect of Inlet Cycle Width on Discharge Capacity:

With an increase in the width of the inlet cycle, water entering the inlet valves experienced reduced energy loss, resulting in an increased area of the inlet flow and enhanced discharge capacity. However, the increase in the width of the input key led to a decrease in the width of the output key, assuming the total width of the weir is kept constant. This resulted in increased local submersion of the output keys (especially at the top of the output key) and a decrease in the discharge capacity of the output key. Therefore, maintaining a balance between the width of the input key and the width of the output key is essential. Observing the results, especially in the comparison between PKW1.4 and PKW1.2 weirs, it was noted that PKW1.2 exhibited better performance across different H/P ratios. Based on previous research results and Anderson's findings, the W_i/W_o=1.20 ratio was selected to examine the impact of the base nose shape. Comparing the outcomes of this study with Anderson's research [20] and graphical analyses conducted in the numerical method of this study showed that the presence of a nose-shaped base under the weir exit keys had a notable effect on flow behavior. It resulted in higher discharges and discharge coefficients compared to weir models lacking this component. As a result, in the design of new piano key weir models, the nose-shaped base was retained, with only cosmetic alterations made to its appearance.

4. Numerical Simulation in Flow 3D:

After determining the shape and dimensions of the nose base for PKW1.2, PKW1.2CL, PKW1.2TR, and PKW1.2S weirs, the flow and its dynamics over the PKW were simulated using the FLOW 3D numerical model, with results compared against laboratory findings to evaluate the model's accuracy. Initial geometric details of the weir were crafted in SketchUp, then converted to the Flow 3D environment via STL files. Meshing, a critical step for model precision, was carefully adjusted based on parameters like the rating curve to minimize errors and maximize result fidelity. This comparative analysis highlighted the significance of precise mesh refinement, capturing the attention of both engineers and researchers. Mesh optimization, achieved through iterative refinement, allowed the hydraulic flow rates in the simulation to closely match those observed in the experimental setup. The final mesh structure, refined through this iterative process, consisted of approximately 2,500,000 cells, providing a detailed and comprehensive analysis within the Flow 3D software.

Table (3) Choosing the number of mesh cells of the numerical model.

Mesh Number	Mesh upstream block	Mesh midstream block	Mesh downstream block	Time (hr)	RMSE	R^2	MAE
Meshing 1	300,000	1,000,000	200,000	12	0.0006	0.9505	0.0041
Meshing 2	**300,000**	**2,000,000**	**200,000**	**14**	**0.0004**	**0.9884**	**0.0011**
Meshing 3	300,000	3,000,000	300,000	19	0.0003	0.9796	0.0023

Simultaneously, the numerical simulation framework involved partitioning the weir into three distinct blocks: upstream, midstream, and downstream segments. This segmentation strategy was designed to replicate laboratory conditions faithfully, enhance spatial resolution, precisely define structural features, and accurately model fluid dynamics. Each delineated block was assigned customized cell counts to ensure specific spatial resolutions. Boundary conditions were meticulously set up to enable smooth information exchange across shared interfaces, with ambient atmospheric conditions and structural boundaries carefully defined.

Table (4) Boundary conditions for the numerical model.

Names Block	Local	boundary condition	Reason for selection
Upstream Block	Xmin	Volume flow rate	Entering the flow as the initial condition
	Xmax	pressure	connection with the atmosphere
	Ymin	Symmetry	Maintaining symmetry conditions
	Ymax	Symmetry	Maintaining symmetry conditions
	Zmin	Wall	Rigid weir floor
	Zmax	pressure	connection with the atmosphere
Midstream Block	Xmin	Volume flow rate	Entering the flow
	Xmax	pressure	connection with the atmosphere
	Ymin	Symmetry	Maintaining symmetry conditions
	Ymax	Symmetry	Maintaining symmetry conditions
	Zmin	Wall	Rigid weir floor
	Zmax	pressure	connection with the atmosphere
Downstream Block	Xmin	Volume flow rate	Entering the flow
	Xmax	pressure	connection with the atmosphere
	Ymin	Symmetry	Maintaining symmetry conditions
	Ymax	Symmetry	Maintaining symmetry conditions
	Zmin	Wall	Rigid weir floor
	Zmax	pressure	connection with the atmosphere

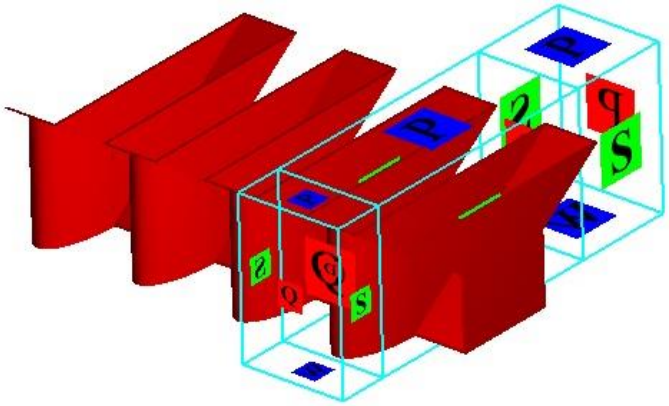

Figure (7) Constructed numerical model, designed model and meshing method.

The choice of the Reynolds-averaged Navier-Stokes (RANS) modeling, specifically the RNG turbulence model, was based on its versatile applicability and proven effectiveness in hydraulic engineering applications. Modeling parameters such as gravitational acceleration, atmospheric pressure, and fluid temperature were carefully calibrated to accurately represent real-world conditions. To enhance computational efficiency, the inherent lateral symmetry of the channel was leveraged, allowing overflow simulations to be confined to half-channel widths. Symmetrical boundary conditions were applied along the midstream interface to optimize computational resources while maintaining analytical integrity. Temporal discretization, vital for numerical stability, was automated by the software to achieve temporal resolutions aligned with computational efficiency. Ultimately, the combination of meticulous calibration of mesh parameters, thoughtful selection of turbulence models, and precise boundary condition prescription facilitated a scientifically rigorous approach to weir modeling. The numerical models were solved using the Simorgh supercomputer at Amir Kabir University of Technology, and the data were extracted for analysis.

Table (5) performance evaluation of turbulence transfer models using the metrics MAE, RMSE, and R2.

Turbulence Model Type	R2	RMSE	MAE	TIME (hr)
Single Equation	0.847	0.033	0.031	8
k-ε	0.930	0.025	0.030	10
RNG	**0.989**	**0.001**	**0.002**	**14**
Prandtl Mixing	0.975	0.012	0.003	16
Large Eddy Simulation	0.980	0.001	0.001	20

Based on this evaluation, the RNG model exhibits the best performance with significantly lower MAE and RMSE values and an R2 close to 1, indicating very good agreement with the data. The k-ε model also performs well with relatively low MAE and RMSE values and a high R2 score. The Single Equation model shows moderate performance, while the Prandtl Mixing and Large Eddy Simulation models perform relatively less accurately, with slightly higher MAE and RMSE values and lower R2 scores compared to the RNG and k-ε models.

The analysis was conducted in Flow 3D software under steady flow conditions, ranging from 5 to 80 liters per second for the weirs. Following flow stability in Flow 3D software, discharges corresponding to the inlet heads for the four weirs (PKW1.2, PKW1.2CL, PKW1.2TR, and PKW1.2S) were extracted, and the discharge coefficient was calculated for each discharge based on the standard discharge formula.

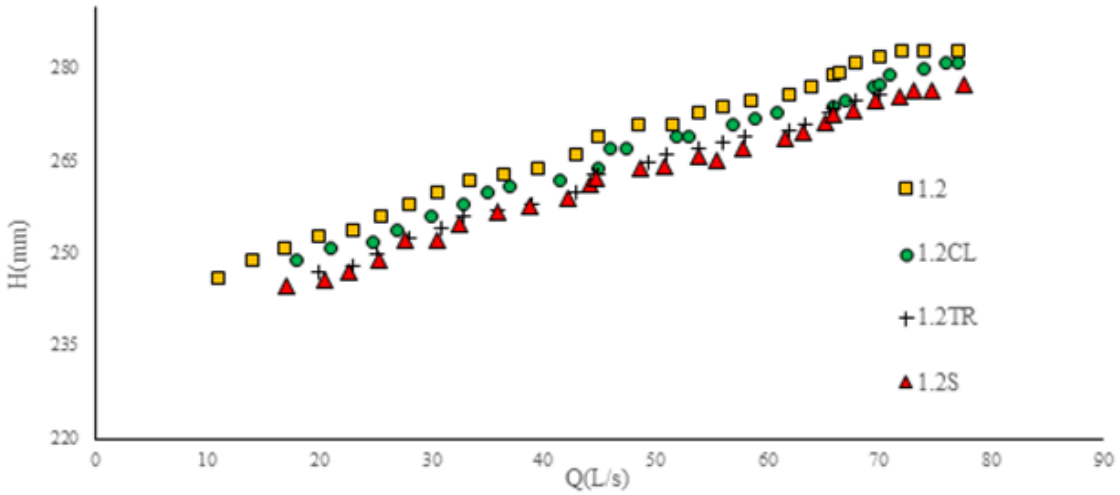

Figure (8): Comparison of rating curve Performance of Piano Key Weirs with Different Nose shape

The figure illustrates the rating curve performance of piano key weirs with different nose bases. Here are the key conclusions drawn from the analysis of the figure:

1. **PKW1.2S vs. PKW1.20 (control weir):**
    - The discharge over the weir with the spindle-shaped PKW1.2S is constant at a lower head compared to the flat-front PKW1.20.
    - The volume of changes in the rating curve is consistent across all three cases.
2. **Overall Efficiency:**
    - PKW1.2S weir demonstrates higher discharge efficiency than the flat nose PKW1.20 weir.
3. **Comparison with Other Nose Bases:**
    - In Figure (9), it is mentioned that the coefficient of discharge in PKW1.2S and PKW1.2TR weirs has increased by 27% and 22%, respectively, compared to the PKW1.20 weir.
    - PKW1.2CL shows an average increase of 10% in the discharge coefficient compared to PKW1.20.

These findings suggest that the spindle shaped nose base (PKW1.2S) contributes to more efficient discharge compared to the flat-front design (PKW1.20). Additionally, PKW1.2S outperforms PKW1.2TR and PKW1.2CL in terms of increased discharge coefficients. The rationale behind this phenomenon lies in the elongation of the front leg of the spindle belt, resulting in a flow trajectory directed further away from the opening of the input keys and exhibiting a milder contour compared to PKW1.2. This disparity accounts for the observed escalation in flow rate and water passage coefficient in the weir under consideration, as opposed to PKW1.2.

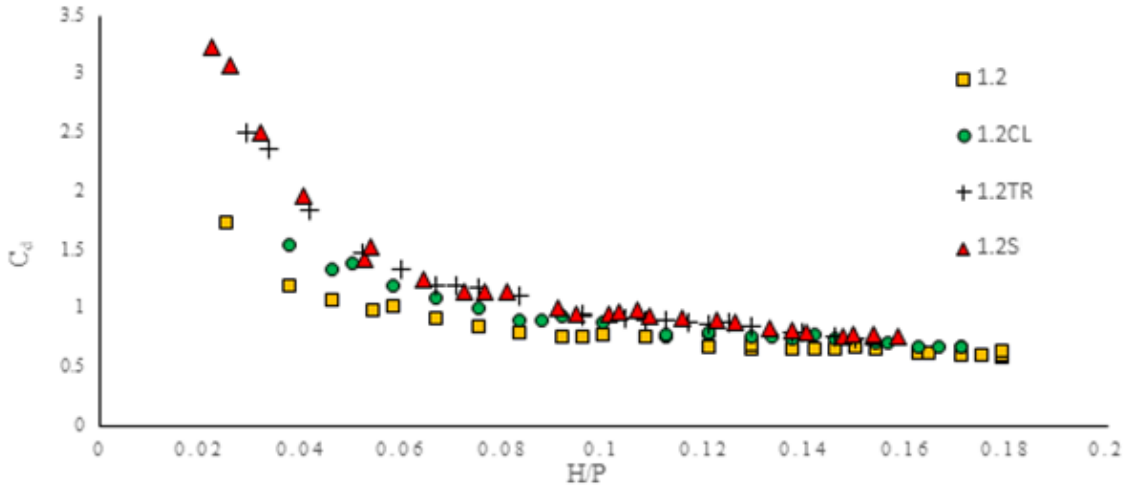

Figure (9): Comparison of discharge Coefficient (C_d) to H/P Ratio in Base weirs with Different Nose shapes in a Three-Dimensional Numerical Model)

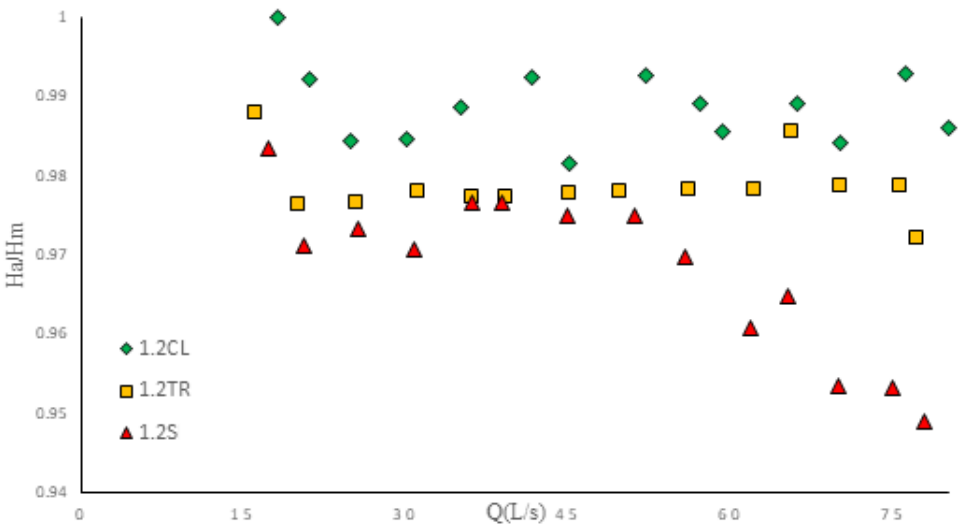

Figure (10): Ratio of head Level in Models with Different Base Nose Shapes to the head Level in the Model with a Flat Nose (PKW1.2)

4.1. Analysis of Downward Trend and Hydraulic Behavior:

The figure illustrates a downward trend in the ratio of flow level compared to the control model (flat nose) across all models. Here is an analysis of the observed trend and its hydraulic implications for different nose shapes:

4.1.1. Flat Nose Model Impact:

The significant downward deviation in the control model (flat nose) is attributed to the nose base of the outlet keys. After hitting the bottom of the outlet keys, the flow undergoes a large and abrupt deviation, leading to a substantial impact on the discharge and a reduction in the volume of incoming water on the discharge keys.

4.1.2. Semi-Cylindrical Nose Model:

In the model with a semi-cylindrical nose, a large deviation and abrupt break in flow occur after hitting the nose, although it is less pronounced than in the flat nose model. The semi-cylindrical shape influences the flow path, contributing to a smoother deviation compared to the flat nose design.

4.1.3. Triangular and Spindle-Shaped Nose Models:

The ratios for triangular and spindle-shaped nose models show a comparatively smoother downward trend. The suggested spindle shape directs the flow towards the input keys with softer lines and less abrupt deviation.

4.1.4. Hydraulic Efficiency:

The smoother flow patterns observed in models with triangular and spindle-shaped noses indicate potential hydraulic efficiency. Reduced flow deviation and smoother transitions contribute to improved discharge efficiency, as observed in the spindle shaped nose weir compared to triangular and semi-cylindrical designs.

4.2. Validation and Error Calculation:

4.2.1. Equations for Error Calculation:

To validate the numerical model data and assess the accuracy of the simulations, several error metrics have been employed. The equations used for error calculation are as follows:

1. **Coefficient of Water Passage (C_d) Error:**

$$E_{cd} = \frac{cd_{NUM} - cd_{EXP}}{cd_{EXP}} \times 100 \quad (4)$$

2. **Head (H) Error:**

$$E_H = \frac{H_{NUM} - H_{EXP}}{H_{EXP}} \times 100 \quad (5)$$

3. **Discharge (Q) Error:**

$$E_Q = \frac{Q_{NUM} - Q_{EXP}}{Q_{EXP}} \times 100 \quad (6)$$

4.2.2. Validation Parameters:

- **R2 (Coefficient of Determination):** Indicates the proportion of the variance in the dependent variable that is predictable from the independent variable.

$$R^2 = 1 - \left[\frac{\sum_{i=1}^{N}(O-P)^2}{\sum_{i=1}^{N} O^2 - \left(\frac{\sum_{i=1}^{N} P^2}{N}\right)}\right] \quad (7)$$

- **MAE (Mean Absolute Error):** Represents the average absolute error between the predicted and observed values.

$$MAE = \frac{1}{N}\sum_{i=1}^{N}|O - P| \quad (8)$$

- **RMSE (Root Mean Squared Error):** Provides the square root of the average of squared differences between predicted and observed values.

$$RMSE = \sqrt{\frac{\sum_{i=1}^{N}(O-P)^2}{N}} \quad (9)$$

Tables (6), (7) and (8): Tables (7) and (8) contain comprehensive information about the percentage errors and validation metrics, allowing a detailed assessment of the agreement between numerical model data and laboratory samples. Table (6) shows the data related to the physical and numerical model and the specific error of each experimenter.

4.2.3. Interpretation

- **Percentage Errors:** Positive or negative values indicate overestimation or underestimation of the numerical model compared to laboratory results.
- **Validation Metrics:** R2, MAE, and RMSE offer quantitative measures of the goodness of fit between numerical and laboratory data.

Table (6) the data related to the physical and numerical model and the specific error of each experimenter

Weir	Simulation number	Physical model			Numerical model			ERROR (%)		
		Q	H	C_d	Q	H	C_d	E_Q	E_H	E_{Cd}
PKW 1	1	0.010	0.011	0.635	0.011	0.012	0.640	11.160	6.818	0.689
	2	0.020	0.017	0.661	0.021	0.017	0.670	5.363	2.647	1.314
	3	0.030	0.024	0.591	0.031	0.024	0.604	2.818	0.417	2.179
	4	0.050	0.036	0.537	0.051	0.036	0.557	1.631	-1.389	3.785
	5	0.080	0.056	0.442	0.080	0.055	0.463	0.550	-2.679	4.730
PK 1.20	1	0.011	0.006	0.735	0.011	0.008	0.905	-2.328	-7.520	9.824
	2	0.020	0.013	0.989	0.020	0.013	0.968	-1.231	0.578	-2.082
	3	0.031	0.020	0.803	0.029	0.020	0.777	-5.673	-1.696	-3.221
	4	0.051	0.031	0.685	0.051	0.032	0.652	-0.685	2.875	-4.819
	5	0.080	0.046	0.594	0.078	0.044	0.627	-2.086	-4.891	5.564
PKW1.40	1	0.011	0.013	0.554	0.011	0.012	0.610	0.951	-5.662	10.173
	2	0.020	0.020	0.518	0.019	0.019	0.535	-2.513	-3.700	3.160
	3	0.030	0.027	0.496	0.029	0.026	0.515	-2.008	-3.867	3.963
	4	0.050	0.037	0.515	0.050	0.036	0.536	-0.005	-2.605	4.034
	5	0.079	0.055	0.449	0.078	0.056	0.432	-1.725	1.345	-3.675
PKW0.71	1	0.013	0.012	0.725	0.014	0.013	0.852	18.292	7.625	14.590
	2	0.020	0.014	0.885	0.020	0.015	0.801	-1.275	6.007	-9.547
	3	0.030	0.022	0.674	0.030	0.023	0.647	0.050	2.823	-4.042
	4	0.050	0.035	0.560	0.051	0.035	0.560	1.000	0.614	0.076
	5	0.080	0.058	0.420	0.080	0.058	0.416	-0.263	0.379	-0.827
PKW0.83	1	0.012	0.014	0.531	0.012	0.015	0.498	0.432	4.667	-6.210
	2	0.020	0.021	0.482	0.021	0.022	0.460	3.562	5.513	-4.447
	3	0.030	0.027	0.496	0.031	0.029	0.473	4.345	6.154	-4.596
	4	0.050	0.042	0.430	0.051	0.040	0.461	1.215	-3.671	7.055
	5	0.073	0.058	0.380	0.082	0.057	0.444	2.824	-1.849	5.744
PKW1.2CL	1	0.013	0.009	1.116	0.014	0.010	0.947	4.231	14.711	-15.163
	2	0.021	0.011	1.334	0.021	0.014	0.946	-1.905	24.127	-29.067
	3	0.030	0.016	1.087	0.029	0.018	0.880	-3.733	12.250	-19.054
	4	0.052	0.029	0.772	0.051	0.030	0.704	-1.952	4.966	-8.826
	5	0.080	0.042	0.681	0.079	0.040	0.727	-0.838	-4.762	6.692
PKW1.2TR	1	0.012	0.005	2.488	0.015	0.006	2.849	14.159	13.872	-6.053
	2	0.020	0.007	2.503	0.020	0.008	2.191	-1.456	8.217	-12.464
	3	0.031	0.014	1.329	0.031	0.014	1.345	-0.251	-0.973	1.224
	4	0.051	0.026	0.892	0.051	0.026	0.871	-0.057	1.505	-2.271
	5	0.077	0.038	0.762	0.078	0.038	0.773	1.677	0.132	1.476

Table (7) error percentage of the studied data in the three-dimensional physical and numerical Model

MODEL	**1**	**2**	**3**	**4**	**5**	**6**	**7**
ERROR (%)	PKW1	PKW1.2	PKW1.4	PKW0.71	PKW0.83	PKW1.2CL	PKW1.2TR
EQ(AVERAGE)	4.304	-2.401	-1.060	3.561	2.476	-0.839	2.814
EH(AVERAGE)	1.163	-2.131	-2.898	3.490	2.163	10.258	4.550
EC_d(AVERAGE)	2.539	1.053	3.531	0.050	-0.491	-13.084	-3.618

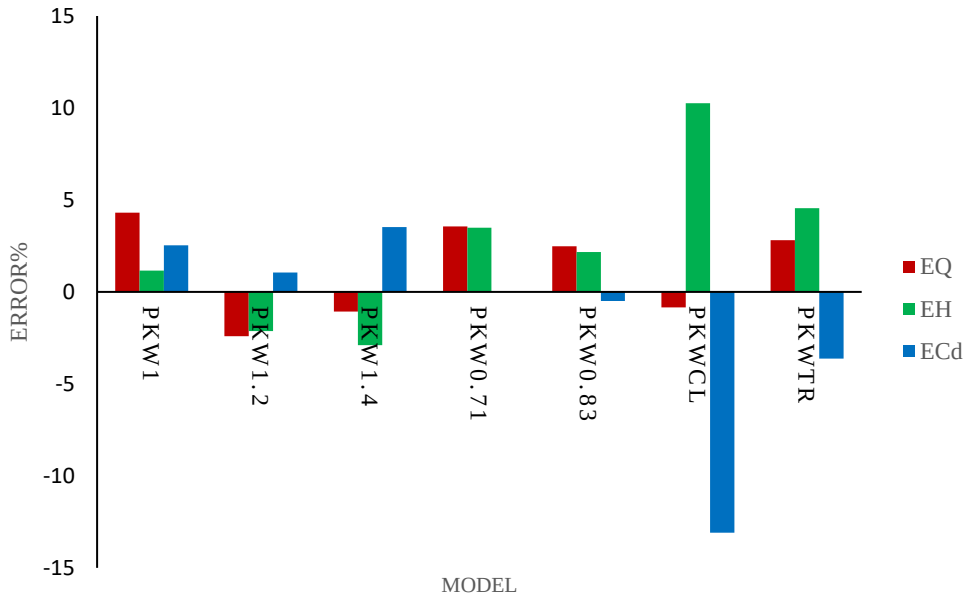

Figure (11) Error percentage of water flow coefficient, discharge and flow head in weirs number 1 to 7 similar to table (2)

Figure (11) illustrates that the Flow 3D three-dimensional model exhibited a low error range, successfully simulating the flow characteristics, including discharge, flow head, and discharge coefficient related to piano key weirs. The small errors observed can be attributed to the role of the boundary layer and the adherence of the flow to the weir body, which may introduce errors in this area, serving as the primary factor in the mentioned results.

Table (8) validation of the studied data in the three-dimensional physical and numerical model

VALIDATION	**PKW1**	**PKW1.2**	**PKW1.4**	**PKW0.71**	**PKW0.83**	**PKW1.2CL**	**PKW1.2TR**
RMSE(Q)	0.0003	0.0004	0.0002	0.0007	0.0007	0.0003	0.0004
RMSE(H)	0.0002	0.0004	0.0003	0.0002	0.0005	0.0008	0.0002
RMSE(C_d)	0.0051	0.0323	0.0113	0.0279	0.0077	0.0872	0.0652
MAE(Q)	0.0001	0.0001	0.0001	0.0002	0.0003	0.0001	0.0001
MAE(H)	0.0001	0.0001	0.0001	0.0001	0.0002	0.0003	0.0002
MAE(C_d)	0.0016	0.0092	0.0038	0.0072	0.0027	0.0292	0.0182
R2(Q)	0.9786	0.9979	0.9927	0.9981	0.9982	0.9896	0.9941
R2(H)	0.9895	0.9875	0.9932	0.9976	0.9887	0.9936	0.9871
R2(C_d)	0.9822	0.9792	0.9962	0.9889	0.9982	0.9532	0.9531

The results of validating the three-dimensional numerical model data indicate that the closer the numerical values of RMSE and MAE are to zero and the numerical value of R2 is to one, the more accurate the model's predictions. It's important to note that RMSE and MAE reflect the magnitude of model error, while R2 signifies the model's efficiency. As shown in Table (6) and in line with the concepts of RMSE, MAE, and R2, the data obtained from the Flow 3D software reveal a strong correlation coefficient (R2), low mean absolute error (MAE), and root mean square error (RMSE) when compared to the laboratory sample data. This suggests that, overall, the numerical method (CFD) can be considered a reliable substitute for laboratory research [21].

4.3. Investigating the Stream Line

After obtaining results from the Flow 3D software simulations and validating the data against the physical model using Tec Plot software, critical information was extracted. This included velocity, pressure, and Stream Line, specifically focusing on the midstream block where overflow occurs. These parameters were analyzed in both two-dimensional and three-dimensional formats across various orientations, using outputs from the simulated models.

To more effectively analyze the impact of the nose design on the weir performance of the PKW, a comparative study was conducted. Data on Stream Lines, pressure, and velocity were examined for the control weir (PKW1.2 with a flat nose shape) and compared with models featuring different nose shapes designs: PKW1.2CL, PKW1.2TR, and PKW1.2S. These comparisons were made in both 2D and 3D layers to provide a comprehensive understanding of the variations.

To logically analyze the flow changes in the two newly designed weirs, we first examined the shape of the Stream Lines around the keys and near the nose. For this purpose, velocity values in the x-direction were extracted in both 2D and 3D formats across three different depth layers. This data helped in visualizing the Stream Lines. Given the structural symmetry, for better visualization of these Stream Lines, they are depicted over a cycle that includes two inlet half-keys and one outlet key.

Figure 11 illustrates these Stream Lines at three different depths: 6, 14, and 20 cm from the base, corresponding to a flow rate of 78 liters per second. Additionally, Figure 11 presents 3D renderings of the velocity contours in the x-direction at these specified depths for models with different nose designs. Additionally, in these figures, the background color represents the velocity at the specified depth, with the x-axis indicating speed in meters per second. Figures 12 and 13 provide detailed views of the four overflow types – PKW1.2, PKW1.2CL, PKW1.2TR, and PKW1.2S – as previously introduced in Figure 2. These figures specifically illustrate the Stream Lines at a depth of 15 cm from the base. The flow rates examined in these scenarios are 30 and 78 liters per second, respectively, allowing for a comparative analysis across different flow conditions.

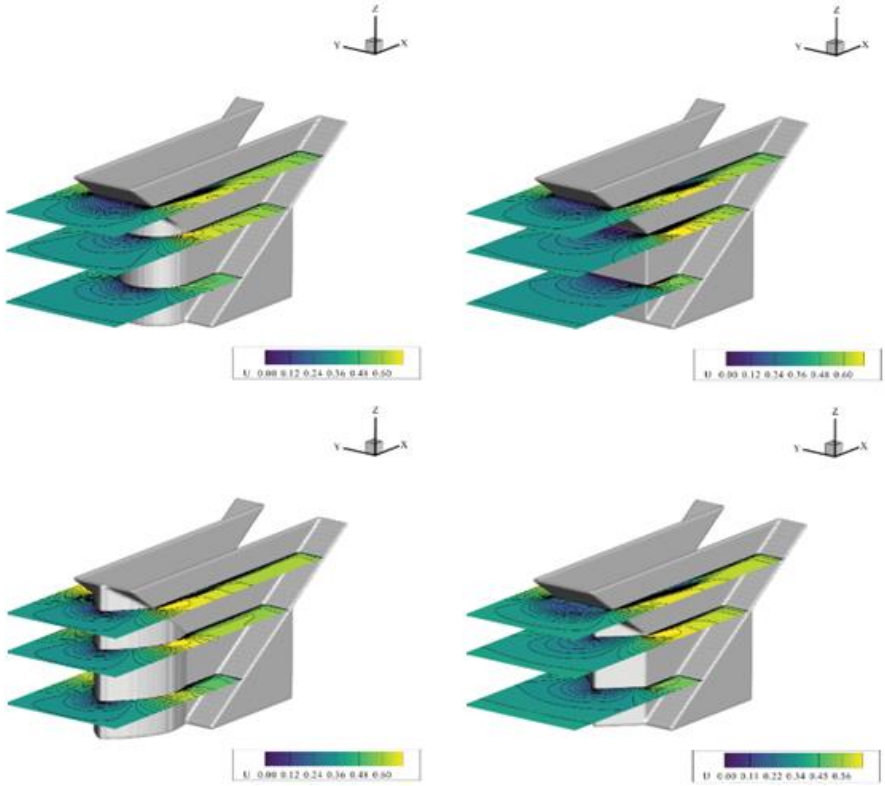

Figure (12): Velocity Contour Profiles at Depths of 6 cm, 14 cm, and 20 cm from the Base, Measured at a Flow Rate of 78 Liters per Second.

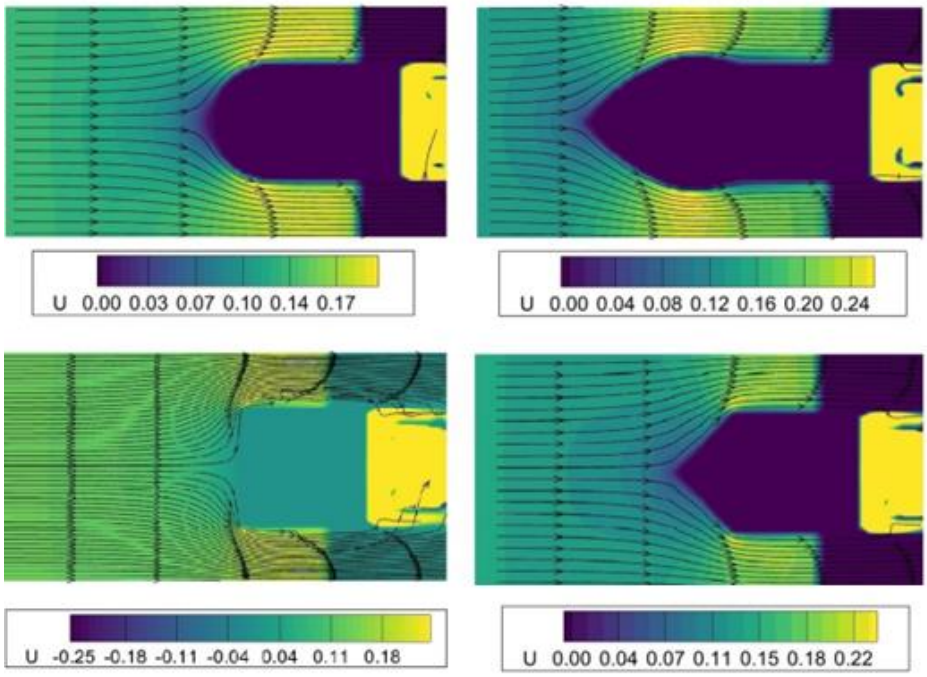

Figure (13): Stream Lines and Velocity Contours for the Model with Different Base Nose shapes, Illustrated at a Depth of 14 cm from the Base and a Flow Rate of 30 Liters per Second.

The observations from Figures 12 and 13 indicate notable differences in flow behavior across the four overflow models. In the PKW1.2 model, the flow experiences a sudden and significant deviation upon striking the flat nosed outlet key. This deviation is much sharper almost 90 degrees compared to the other models, leading to a substantial reduction in the volume of water passing over the weir switches.

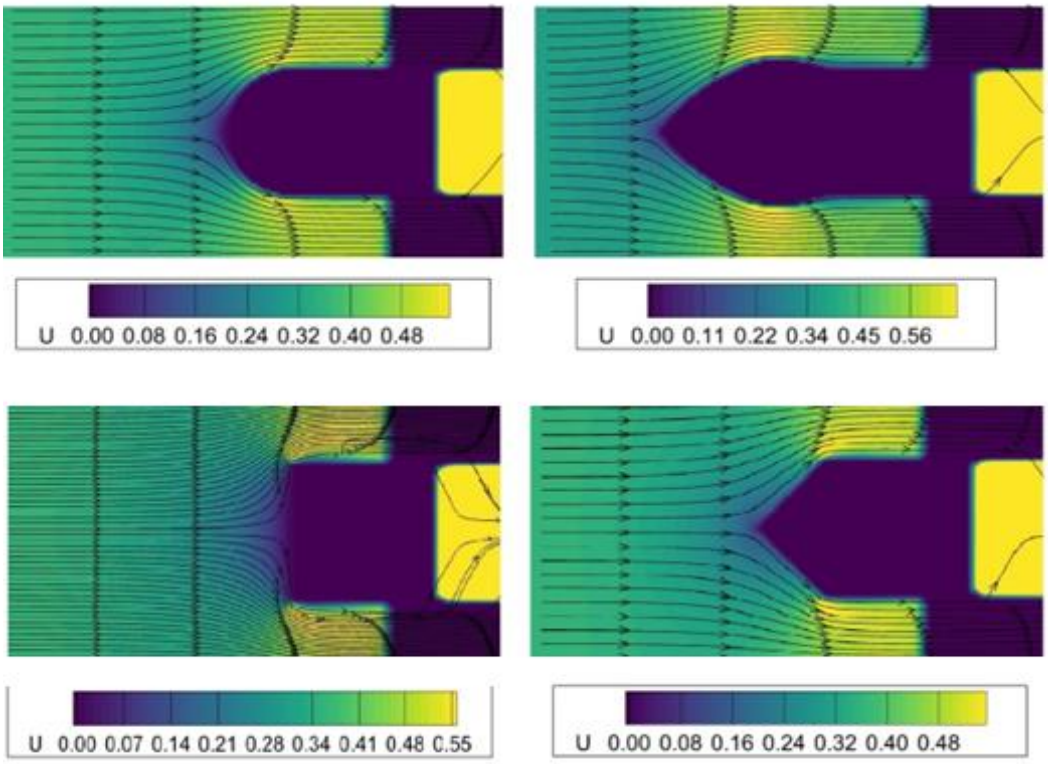

Figure (14): Stream Lines and Velocity Contours for the Model with Different base Nose shapes, Displayed at a Depth of 14 cm from the Base, at a Flow Rate of 78 Liters per Second.

In contrast, the PKW1.2CL model, with its semi-cylindrical nose, causes the flow to deviate considerably, resulting in disrupted Stream Lines. This effect is less pronounced in the spindle and triangular-nosed models (PKW1.2S and PKW1.2TR), where the flow is directed towards the inlet keys with smoother lines and fewer disturbances. This characteristic significantly contributes to an increased flow rate and higher water passage coefficient in the PKW1.2S and PKW1.2TR models compared to the PKW1.2CL and PKW1.2. Furthermore, as illustrated in Figure 12, the flow velocity plays a significant role in influencing the nose shape's impact on the flow. In the case of the PKW1.2S model, there is a noticeable trend: the Stream Lines show minimal deviation, and the velocity in the x-direction is comparatively higher. This suggests that the specific design of the PKW1.2S model's nose contributes to a more Streamlined flow, with less disturbance and increased speed.

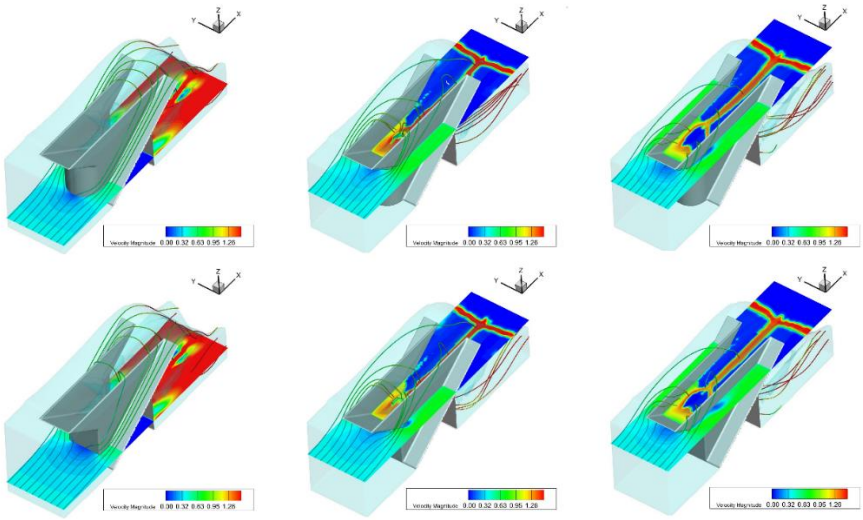

Figure (15): Stream Lines and Contours of Average Flow Velocity in Models with Flat and Semi-Cylindrical Nose shapes, Illustrated at Depths of 6 cm, 14 cm, and 20 cm from the Base, at a Flow Rate of 78 Liters per Second.

Figure 15 reveals that in the PKW1.2 and PKW1.2CL weirs, there is a sharp and immediate change in the angle of the Stream Lines upon contact with the nose, occurring close to the entrance of the weir inlet keys. This contrasts with the PKW1.2S and PKW1.2TR weirs, where the change in flow direction happens over a longer distance, at a gentler angle, and further from the inlet key entrances. This results in a smoother flow with less turbulence, allowing more water to enter the inlet keys. Additionally, it is observed that in deeper layers, currents pass through the end edge of the outlet switch, whereas in higher layers, they tend to flow over the lateral edge of the overflow. These patterns underscore the significant impact of the nose's design on both the flow trajectory and the point of water descent.

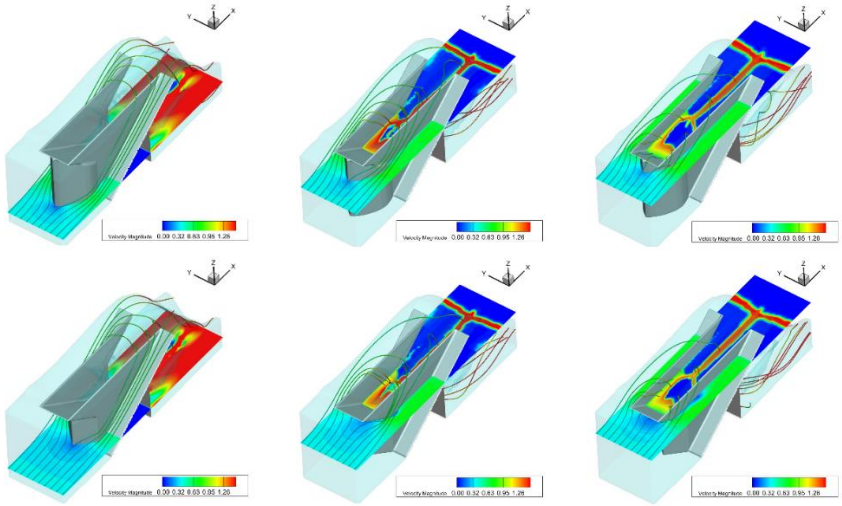

Figure (16): Stream Lines and Contours of Average Flow Velocity in Models with Triangular and Spindle Nose shapes, Presented at Depths of 6 cm, 14 cm, and 20 cm from the base, at a Flow Rate of 78 Liters per Second.

In Figure 16, the model with a spindle nose shows less mixing of the flow near the lateral edge of the passage, which facilitates a higher volume of water flow through this type of weir. A similar observation can be seen in Figure 17, further supporting this conclusion.

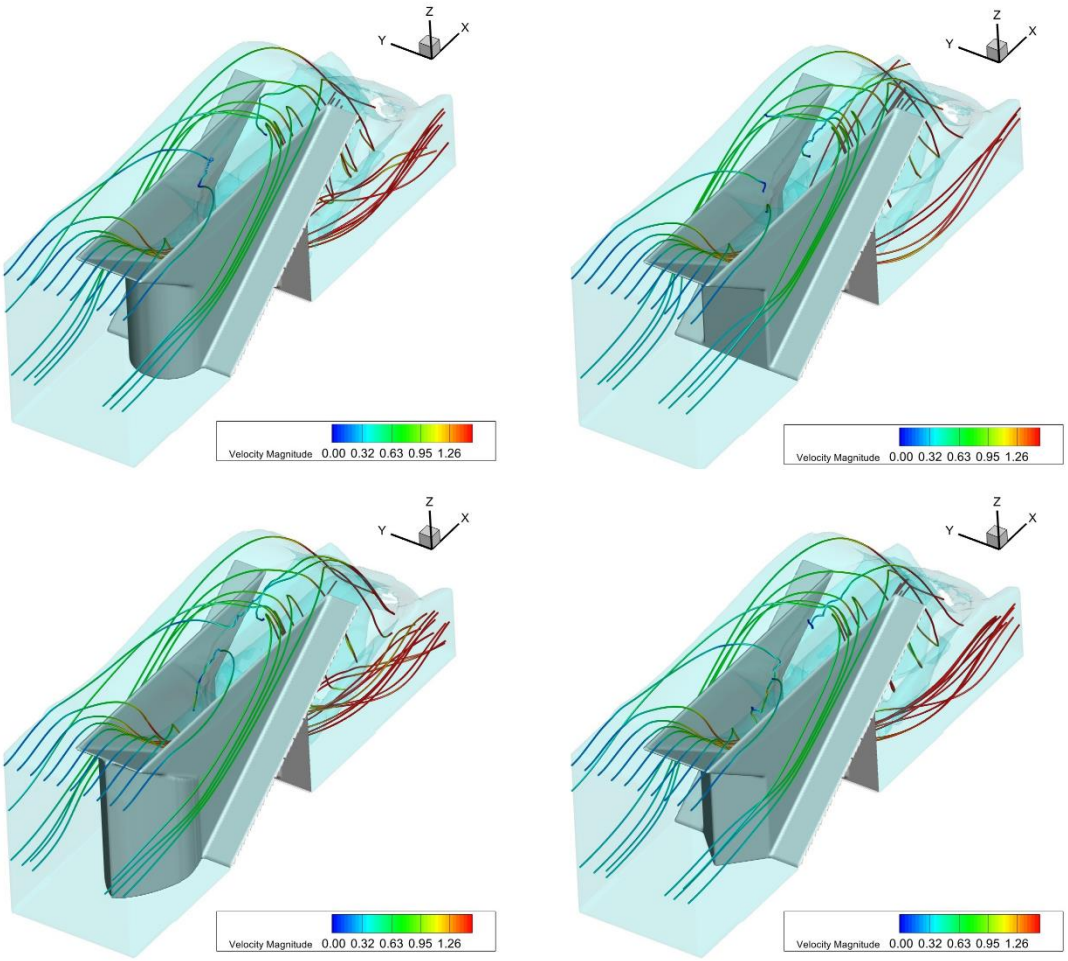

Figure (17): Stream Lines Indicating Average Flow Speed in the Model with Various Nose shapes, Measured at Mid-Depth and at the Flow Surface Level, at a Flow Rate of 78 Liters per Second.

Figure 17's depiction of the eddies in the PKW1.2 and PKW1.2CL weirs indicates significant turbulence immediately following the flow's passage through the keys. In contrast, the PKW1.2TR and PKW1.2S weirs exhibit considerably less turbulence post-key passage, contributing to the enhanced flow capacity of these two designs.

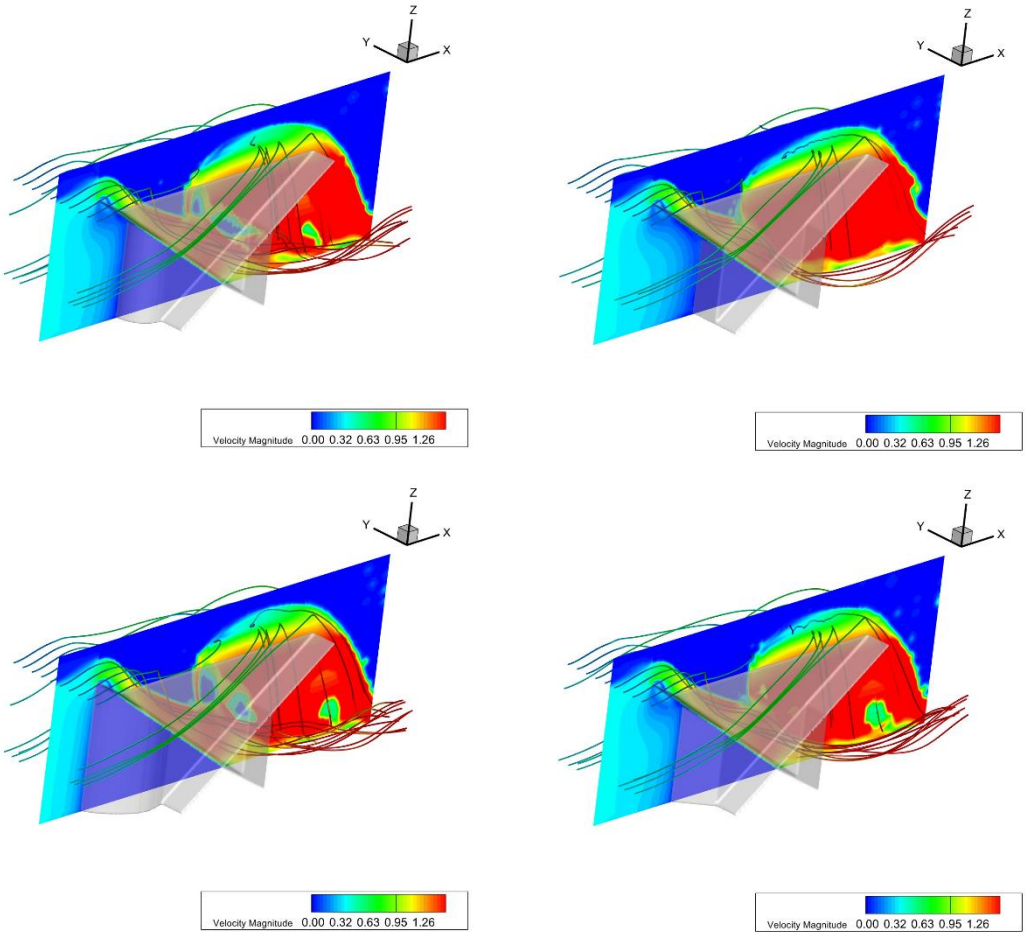

Figure (18): Cross-Sectional View of Stream Lines and Contours Representing Average Flow Velocity in Models with Various Nose shapes, Focused at the Center of the Nose, at a Flow Rate of 78 Liters per Second.

In Figure 18, an examination of the Stream Lines in the cross-section reveals that the flow in models with spindle and triangular noses experiences less mixing. The point where the flow separates from the nose's body in these models occurs with minimal energy friction and reduced speed, which increases the flow rate and discharge Coefficient and decreases the level of water on the weir. This is in stark contrast to the flat nosed model, where the separation point is marked by the greatest deviation, speed reduction, and energy loss.

4.4. Investigating the Pressure Parameter

The study revealed notable differences in pressure distribution across various piano key weir (PKW) designs. In PKW1.2S and PKW1.2TR models, the pressure difference on the output keys is lower compared to that in PKW1.2CL and PKW1.2 models. This observation aligns with the principle that a smaller pressure difference facilitates greater flow through the exit keys. While there are slight variations in pressure at the top of the noses in PKW1.2S and PKW1.2TR models, the significant pressure difference at the head of these overflows can also influence the discharge due to the presence of a nose.

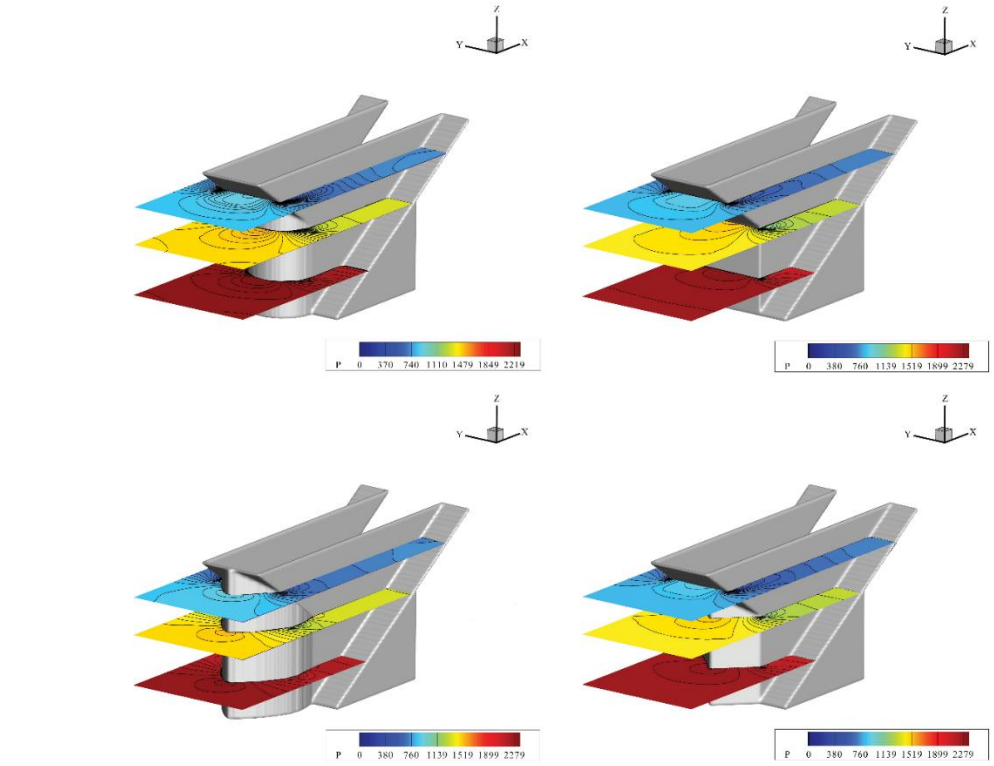

Figure (19): Pressure Contours at Depths of 6 cm, 14 cm, and 20 cm from the base, at a Flow Rate of 78 Liters per Second.

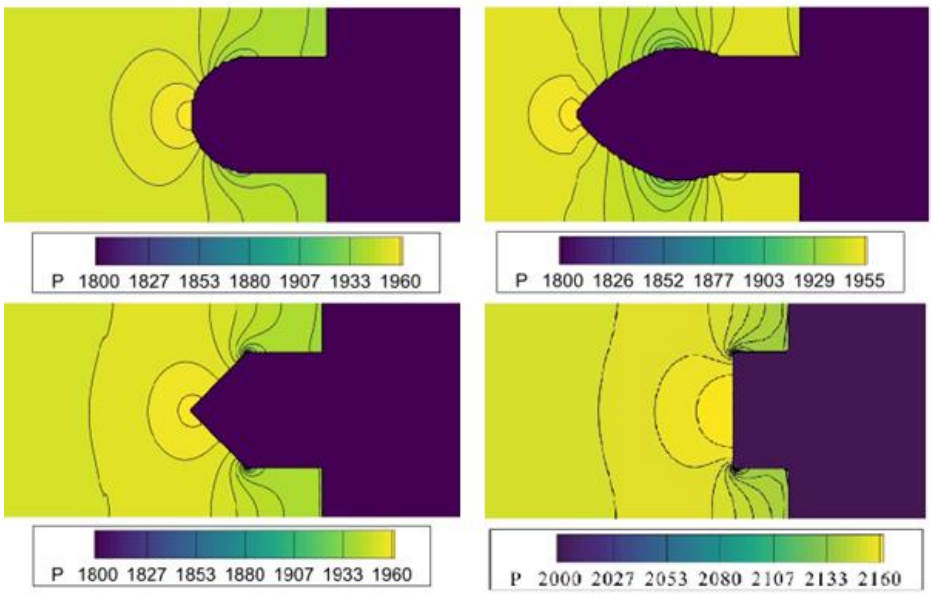

Figure (20): Pressure Contours at a Depth of 6 cm from the base, Measured at a Flow Rate of 30 Liters per Second.

According to the pressure lines in Figure 20, the unique shape of the nose in the PKW1.2S model (characterized by extended legs and a lower angle at the tip) results in lower pressure at the tip compared to other models, contributing to its higher efficiency. The results highlighted those models with semi-cylindrical and flat noses experienced significant flow deviation and abrupt disruption post-impact with the nose. This effect was markedly reduced in models with triangular and spindle-shaped noses.

5. Conclusion

This study investigated the influence of the nose shape of piano key weirs on flow hydraulics, utilizing both laboratory and numerical models. The numerical modeling was conducted using FLOW 3D software. Validation of the three-dimensional numerical model data indicated a high degree of accuracy, with RMSE and MAE values approaching zero and an R^2 value close to one. These findings suggest that computational fluid dynamics (CFD) can effectively supplement laboratory research. The results highlighted those models with semi-cylindrical and flat noses experienced significant flow deviation and abrupt disruption post-impact with the nose. This effect was markedly reduced in models with triangular and spindle-shaped noses. Notably, the spindle shaped design directed the flow towards the inlet keys with smoother transitions and less fragmentation. This characteristic was a key factor in enhancing discharge efficiency in the spindle nosed weirs compared to the flat and semi-cylindrical designs.

Reference

1. Chow, V.T. (1959). "Open channel hydraulics." McGraw-Hill Book Company, New York, NY.
2. Ouamane, A., and Lempérière, F. (2006). "Design of a new economic shape of weir." Proc., Intl. Symp. on Dams in the Societies of the 21st Century, 463-470, Barcelona, Spain.
3. Crookston, B. M., Anderson, A., Shearin-Feimster, L., and Tullis, B. P. (2014). "Mitigation investigation of flow-induced vibrations at a rehabilitated spillway." Proc., 5th IAHR Intl. Symp. on Hydraulic Structures, Univ. of Queensland Brisbane, Brisbane, Australia.
4. Machiels, O. (2012). "Experimental study of the hydraulic behaviour of Piano Key Weirs." Ph.D. Dissertation, Faculty of Applied Science, University of Liège, Liège, Belgium.
5. Blanc, P., and Lempérière, F. (2001). "Labyrinth spillways have a promising future." Intl. J. of Hydropower and Dams, 8(4), 129-131.
6. Muslu, Y. (2001). "Numerical analysis for lateral weir flow." J. of Irrigation and Drainage Eng., ASCE, 127, 246.
7. Erpicum, S., Machiels, O., Dewals, B., Pirotton, M., and Archambeau, P. (2012). "Numerical and physical hydraulic modeling of Piano Key Weirs." Proc., ASIA 2012 - 4th Intl. Conf. on Water Resources and Renewable Energy Development in Asia, Chiang Mai, Thailand.
8. Tullis, J.P., Amanian, N., and Waldron, D. (1995). "Design of Labyrinth Spillways." J. of Hydraulic Eng., ASCE, 121.
9. Lux, F.L., and Hinchcliff, D. (1985). "Design and construction of labyrinth spillways." Proc., 15th Intl. Congress on Large Dams, ICOLD, Vol. 4, 249-274, Paris, France.
10. Erpicum, S., Laugier, F., Ho to Khanh, M., & Pfister, M. (2017). Labyrinth and Piano Key Weirs III–PKW 2017. CRC Press, Boca Raton, FL.
11. Kabiri-Samani, A., and Javaheri, A. (2012). "Discharge coefficient for free and submerged

flow over Piano Key weirs." Hydraulic Research J., 50(1), 114-120.
12. Hien, T.C., Son, H.T., and Khanh, M.H.T. (2006). "Results of some piano Key weirs hydraulic model tests in Vietnam." Proc., 22nd ICOLD Congress, CIGB/ICOLD, Barcelona, Spain.
13. Laugier, F., Lochu, A., Gille, C., Leite Ribeiro, M., and Boillat, J-L. (2009). "Design and construction of a labyrinth PKW spillway at St-Marc Dam." Hydropower and Dams J., 15(5), 100-107.
14. Cicero, G.M., Menon, J.M., Luck, M., and Pinchard, T. (2011). "Experimental study of side and scale effects on hydraulic performances of a Piano Key Weir." In: Erpicum, S., Laugier, F., Boillat, J-L, Pirotton, M., Reverchon, B., and Schleiss, A-J (Eds.), Labyrinth and Piano Key Weirs, 167-172, CRC Press, London.
15. Pralong, J., Vermeulen, J., Blancher, B., Laugier, F., Erpicum, S., Machiels, O., Pirotton, M., Boillat, J.L, Leite Ribeiro, M., and Schleiss, A.J. (2011). "A naming convention for the piano key weirs geometrical parameters." In: Erpicum, S., Laugier, F., Boillat, J-L, Pirotton, M., Reverchon, B., and Schleiss, A-J (Eds.), Labyrinth and Piano Key Weirs, 271-278, CRC Press, London.
16. Denys, F. J. M., and Basson, G. R. (2018). "Transient hydrodynamics of Piano Key Weirs." Proc., 7th IAHR Intl. Symp. on Hydraulic Structures, ISHS2018, 518-527, DigitalCommons@USU, Logan, UT.
17. Anderson, A., and Tullis, B. P. (2018). "Finite crest length weir nappe oscillation." J. of Hydraulic Eng., ASCE, 144(6), 04018020. https://doi.org/10.1061/(ASCE)HY.1943-7900.0001461
18. Erpicum, S., Laugier, F., Boillat, J.-L., Pirotton, M., Reverchon, B., and Schleiss, A. J. (2011). "Labyrinth and Piano Key Weirs–PKW 2011." CRC Press, Boca Raton, FL.
19. Aydin, C.M., and Emiroglu, M.E. (2011). "Determination of capacity of labyrinth side weir by CFD." Flow Measurement and Instrumentation, 29, 1-8.
20. Cicero, G.M., Delisle, J.R., Lefebvre, V., and Vermeulen, J. (2013). "Experimental and numerical study of the hydraulic performance of a trapezoidal PKW." Proc., Intl. Workshop on Labyrinths and Piano Key Weirs PKW II 2013, 265-272, CRC Press.
21. Anderson, R. M. (2011). "Piano Key Weir Head Discharge Relationships." Master's Thesis, Utah State University, Logan, Utah.
22. Crookston, B.M., Anderson, R.M., and Tullis, B.P. (2018). "Free-flow discharge estimation method for Piano Key weir geometries." J. of Hydro-environment Research, 19, 160-167.